Complex Permittivity Measurements of Single-walled Carbon Nanotubes at Microwave Frequencies

C. Darne,[1] L-M. Xie,[1] W. Zagozdzon-Wosik,[1] H. K. Schmidt,[2] and J. Wosik[1]

[1]Department of Electrical and Computer Engineering and Texas Center for Superconductivity, University of Houston, Houston, TX, 77204, University of Houston, Houston, TX, 77204; [2]Department of Chemical and Biomolecular Engineering, Smalley Institute for Nanoscale Science & Technology, Rice University, Houston, Texas 77005

ABSTRACT

We report on the high frequency complex permittivity characterization of single-walled carbon nanotubes (SWNT) using broadband and narrowband frequency range techniques. SWNT suspensions, powder and fiber were investigated and the samples were a mixture of semiconducting and metallic nanotubes. Shielded open-circuited coaxial probe (50 MHz to 10 GHz) and dielectric microwave resonators were developed for this project. Two dielectric resonators supporting TE_{011} (3.4 GHz) and TM_{011} (6.5 GHz) modes and one $TE_{01\delta}$ split-post resonator (12 GHz) were employed. An excellent correlation was observed between the values obtained from the coaxial probe and tubular resonator techniques. From our calculations, average conductivities of SWNT and surfactant suspensions were found to be 1.16×10^{5} S/m and 1.66×10^{-2} S/m, respectively. In addition, a split-post dielectric resonator technique was developed to investigate origin of rf/microwave losses in SWNT samples. Resonant frequency and quality-factor Q changes introduced by SWNT interaction with the $TE_{01\delta}$ mode electric and microwave fields were measured. The resulting frequency and quality factor maps allowed to distinguish between electric and/or magnetic fields induced losses.

Keywords: carbon nanotubes, dielectric resonator, coaxial probe, dielectric losses, electrical conductivity

1 INTRODUCTION

Carbon nanotubes have been widely investigated because of their unique electrical, thermal and mechanical properties. The current and potential applications include nano-electronics [1, 2], photo-electronics [3], interconnects [4] and NEMS [5, 6]. One of the emerging nanotubes applications is electromagnetic shielding, in which networks of aligned or randomly distributed SWNT are employed [7, 8]. It was already demonstrated that composites containing SWNT exhibited 49 dB shielding effectiveness at 10 MHz, with 15% NT loading of a polymer composite [9]. These developments require further determination of nanotubes basic physical high frequency properties. Nanotube films are being studied as electrically percolative layers that can provide relatively low percolation thresholds because of their high aspect ratio geometry.

Nanotubes properties also need to be studied for biomedical applications such as cancer therapeutic or contrast enhancement agents [10, 11]. The localized destruction of tumor cells through the heating interaction of nanotubes with rf/microwave operating frequencies is an example of recent advancements. Unlike nanotube composites or films, these samples are suspended using surfactants or require functionalization and hence exhibit different inter-nanotube interactions. Their dielectric and conductivity response is therefore significantly different and is still a subject of research interest.

In this paper, we have made use of specially designed dielectric resonators and modified coaxial probe for enhanced sensitivity measurements of nanotube films and SWNT suspensions. The dielectric resonators are capable of discretely measuring the magnetic and electric response of the samples using spatially varying electromagnetic distribution. The coaxial probe can scan the sample response over a wide frequency range.

2 MEASUREMENT TECHNIQUES

2.1 Dielectric Resonators

Dielectric resonator (DR) usually consists of a disk of ceramic with a large dielectric constant and a low loss tangent. Such resonator can support similar microwave modes as a hollow cavity, however the permittivity change determines the resonator boundaries [12].

DR usually has high quality factors and their design can be specialized for different materials to-be-characterized. Different modes (TE, TM, and HEM) with varying field distributions can be excited in these resonators. Quality factor and resonant frequency shifts for the selected mode should be monitored and used for determining the sample complex permittivity. For this study, we have used two variants of dielectric resonator namely tubular dielectric resonator [13] and split-post dielectric resonator [14].

2.1.1 Tubular Dielectric Resonator

The tubular resonator comprised of a dielectric cylinder with a cylindrical plug removed from the center (Figure 1a). The central hole was used for inserting the samples within the resonator microwave fields. TE_{011} mode was excited and the coupling coaxial cable loops were used. This mode has an in-plane component of the electric field (E_φ) that is zero at the center of the resonator and increases radially outwards.

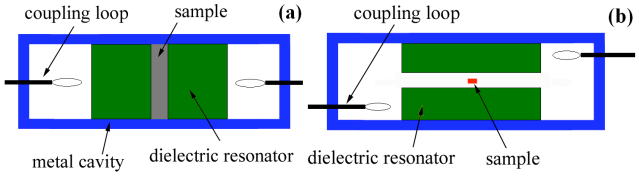

Figure 1: Cross-sectional views of (a) tubular dielectric resonator and (b) split-post dielectric resonator.

TM_{011} mode was excited by a dipol antenna. For the TM_{011} mode, the magnitude of the out-of-plane component of the electric field (E_z) is strongest at the center of the resonator and reduces radially outwards. Hence sample diameter in this case can be small.

The sample was held in a quartz capillary tube, which has a very low microwave dielectric loss. Measurements of both single (s_{11}) and two (s_{21}) ports complex reflection coefficients versus frequency were performed with and without the actual sample. The TE_{011} mode (3.4 GHz) used a 4 mm diameter tube, while the TM_{011} mode (6.1 GHz) had a tube diameter of 0.3 mm.

2.1.2 Split-post Dielectric Resonator (SPDR)

The SPDR design comprised of two parallel dielectric discs separated by a small gap (Figure 1b). The resonator's mode was excited inductively using coupling coaxial cable loops. This resonator supported $TE_{01\delta}$ mode with an azimuthal component of electric field (E_φ) along the radial axis and magnetic field (H_z) along the z-axis.

Electromagnetic modeling of the resonator, based on the perturbation theory, was used for establishing relation between the experimental data and the material parameters. The perturbation theory assumes a local field disturbance within the resonator, and hence the sample volume required for measurements is very small. The sample introduced within the resonator was treated as a part of the resonator and the field disturbance within the resonator was compared with the unperturbed field. The relation between the sample induced frequency shift and real part of permittivity/permeability for the sample was determined as

$$(f_2' - f_1') = -Af_1' \int_V (\overline{E}_1 \cdot \Delta\tilde{\varepsilon}' \overline{E}_1 + \overline{H}_1 \cdot \Delta\tilde{\mu}' \overline{H}_1) dv \qquad (1)$$

where A denotes the calibration factor representing the total energy stored within the resonator. We observe that the change in measured resonant frequency is proportional to the dielectric constant or permeability change for the sample relative to air (vacuum). For a pure dielectric material, the frequency shift is caused by its interaction only with the electric field giving a negative frequency shift. As for permeability, it can be larger or smaller than zero, and thus, the frequency shifts can be positive or negative. The relation between the measured sample loss (1/Q) and imaginary part of complex permittivity/permeability was calculated to be:

$$\frac{1}{Q_2} - \frac{1}{Q_1} = 2A \int_V (\overline{E}_1 \cdot \Delta\tilde{\varepsilon}'' \overline{E}_1 + \overline{H}_1 \cdot \Delta\tilde{\mu}'' \overline{H}_1) dv \qquad (2)$$

The resonator was electromagnetically modeled based on dielectric rod waveguide model proposed by Itoh and Rudokas [14]. The field distributions over the center plane of a dielectric cylinder resonator were calculated and we assumed that the same field distributions existed in the small air-gap within the SPDR. The tangential components of electric and magnetic fields were continuous across the dielectric interface as seen in the Figures 2a and 3a.

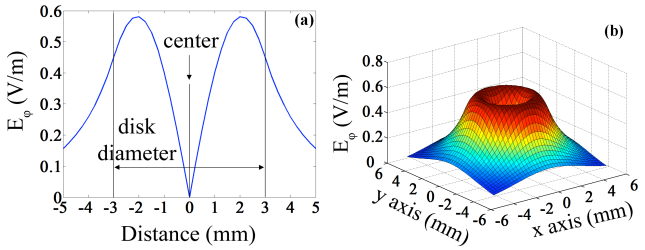

Figure 2: (a) shows the 2D plot of electric (E_φ) field distribution within SPDR as a function of the disk diameter, (b) shows 3D map.

E_φ has zero field strength at the center of the resonator and increases radially outwards. The magnetic field (H_z) component, however, has a maximum field strength at the center of the resonator. Three dimensional electric and magnetic field distribution plots are shown in Figures 2b and 3b. The field outside the resonator was evanescent in nature and decay slowly. Thus, a sample within the resonator experiences strong electric field away from the center of the resonator while the magnetic field interaction is strongest at the center. The sample response to the field distribution helps us to quantify it as a pure dielectric/metal or a combination of the both.

Based on the cavity perturbation method, we were able to measure small sample volumes permittivity by scanning them in a meandering fashion within the resonator.

NSTI-Nanotech 2009, www.nsti.org, ISBN 978-1-4398-1782-7 Vol. 1, 2009

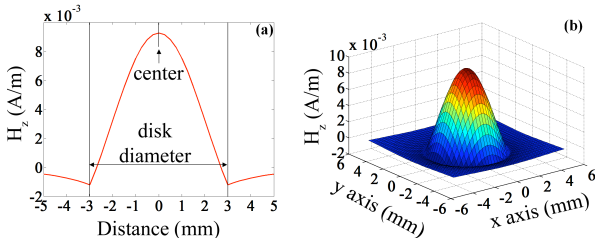

Figure 3: (a) shows the 2D plot of magnetic (H_z) field distribution within SPDR as a function of the disk diameter, (b) shows 3D map.

The scanning was performed using a two-axis stepper motor configured through a NI PCI-7342 card and the motion was controlled using NI Motion Assistant software. Vector network analyzer (HP8720) was connected to the resonator using flexible air-line cables, and measured the magnitude of complex forward scattering parameter (s_{21}). A LABVIEW interface was used for acquisition and post-processing of data. Real time averaging and data fitting were performed to reduce the effect of noise and improve the measurement reliability.

2.2 Shielded Open-circuited Coaxial Probe

A sketch of the coaxial sample probe used for broadband measurements is shown in Figure 4. The design consists of a section of coaxial transmission line with the inner conductor shorter in length than the outer conductor. A dielectric bead at the bottom of the air line prevents the liquid sample from leaking out and was designed to match the probe to 50 Ω. The active part of the probe begins on the upper surface of the bead and runs the entire length of the inner conductor, above which the coaxial section turns into a circular waveguide and is terminated in an open circuit. Such probe design ensures that no field leaks out from the open end of the probe [15]. Due to the azimuthal symmetry, only TEM and evanescent TM_{0n} modes are present within the probe. A full-fledged electromagnetic analysis for the coaxial probe is presented in [16].

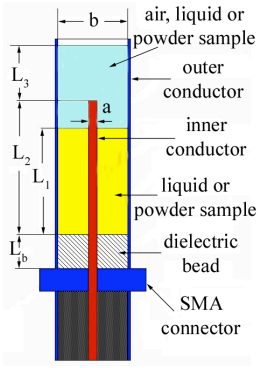

Figure 4: Shielded open-circuited sample holder used for broadband frequency measurements of dielectric liquids and powders.

One port complex reflection coefficient (s_{11}) was measured using vector network analyzer (HP8720) and inverse problem solving technique was used to calculate the complex permittivity. Measurements were also performed on an empty probe to precisely determine the phase rotation across the bead.

3 RESULTS

The SWNT sample was measured over a wide frequency range from 50 MHz to 7 GHz using a coaxial probe. The SWNT were homogeneously suspended in water using surfactant (pluronic). Pluronic powder measurements showed frequency independent dielectric constant (less than 2) along with small dielectric loss. It was therefore concluded that the contribution of pluronic to the SWNT suspension could be neglected.

SWNT suspension and aqueous pluronic solution exhibited identical response for the real part of permittivity. One of the possible reasons for this behavior may be the relatively large dielectric constant of water that screened the response from low density SWNT suspension.

Imaginary part of permittivity for the SWNT suspension was however considerably higher than the aqueous pluronic solution. It was measured for varying SWNT concentrations by diluting the original SWNT suspension with aqueous pluronic solution. The measured imaginary part was found to reduce with dilution thus indicating that the nanotubes were responsible for the loss. Sample conductivity was later extracted from the measured imaginary parts of permittivity for different concentrations. A general expression relating the imaginary part of permittivity to the conductivity is given by $\varepsilon''_{measured} = \varepsilon''_{suspension} + \sigma/\omega\varepsilon_0$, where $\varepsilon''_{measured}$ and $\varepsilon''_{suspension}$ are the total and actual imaginary part of permittivity, σ is the sample conductivity, ω is the angular frequency and ε_0 is the vacuum permittivity. Data fitting was performed to extract the sample conductivity. Conductivity as a function of the normalized sample concentration is shown in Figure 5.

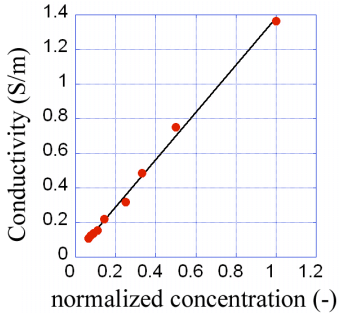

Figure 5: Plot showing sample conductivity as a function of the normalized nanotube concentration.

The calculated conductivity of the aqueous pluronic solution was found to be 1.6587×10^{-2} S/m [17]. Also, using volume fraction calculations for the nanotube suspension an average SWNT conductivity of 1.16×10^{5} S/m was obtained and found to be in agreement with the literature [18].

We also used a low permittivity liquid surfactant (pluronic L10) suspended SWNT for our measurements. The surfactant helped to retain the nanotube homogeneity. Coaxial probe measurements were repeated with this new suspension. A reference run with only surfactant was also measured over the same frequency range. The SWNT suspension was found to show not only a higher dielectric constant as compared to the surfactant (Figure 6a), but also an increased imaginary part of permittivity (Figure 6b).

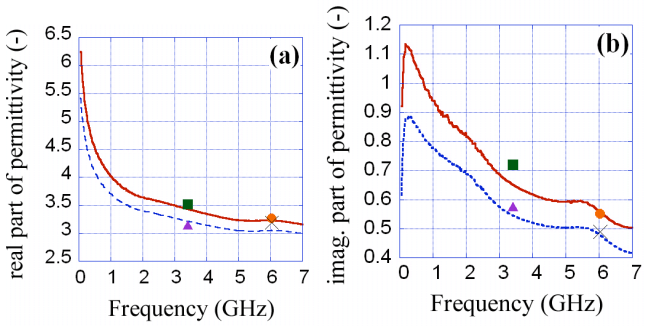

Figure 6: SWNT suspension measured using coaxial probe (solid line) and tubular resonators (TE:■, TM:● modes). Surfactant measured using coaxial probe (dotted line) and tubular resonators (TE: ▲, TM:X modes).

Tubular dielectric resonators with TE_{011} (3.4 GHz) and TM_{011} (6 GHz) modes were also used to measure this SWNT suspension. The results are shown in Figures 6a and 6b. Good correlation was observed between the measurements performed using tubular resonators and coaxial probe. Additional modeling needs to be performed to extract the stand-alone dielectric response of SWNT from the suspension.

Split-post dielectric resonator was used for measuring permittivity of SWNT and also multi-walled carbon nanotube (MWNT) samples. The frequency shift and the sample loss of the latter are shown in Figures 7a and 7b, respectively. Magnetic response was prominent at the center of the resonator while the electric reponse increases away from the center. This result is in contrary to the response observed for SWNT/surfactant films, where no microwave magnetic field interaction was present. Eddy currents induced in the sample and also magnetic losses induced by the iron catalyst particles used for MWNT synthesis contributed towards the central positive frequency shift. The complex permittivity (and permeability) of the sample can be extracted by fitting the measured data to the simulation based on shown earlier in this paper perturbation theory. This resonator technique proved to be very promissing for probing dielectric and magnetic nanotubes properties.

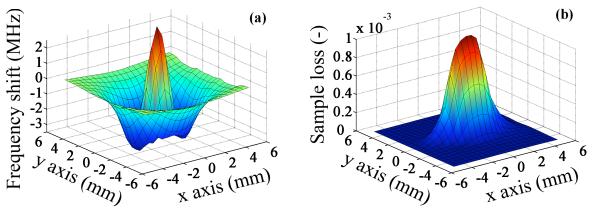

Figure 7: Frequency shift and sample loss for multi-walled carbon nanotubes.

ACNOWLEDGEMENTS

The authors thank Qingkai Yu and Steven S. Pei for providing multi-walled carbon nanotubes film.

REFERENCES

[1]R. H. Baughman, A. A. Zakhidov, W. A. de Heer, Science, 297, 787, 2002.
[2]Z. Yu, P. J. Burke, Nano Letters, Vol. 5, No. 7, 2005, 1403-1406.
[3]M. Freitag, Y. Martin , J. A. Misewich, R. Martel, P. Avouris, Nano Letters, 3, 1067, 2003.
[4]J. J. Plombon, K. P. O'Brien, F. Gstrein, V. M. Dubin, Y. Jiao, Applied Physics Letters, 90, 063106, 2007.
[5]P. G. Collins, K. B. Bradley, M. Ishigamo, A. Zettl, Science, 287, 1801, 2000.
[6]A. B. Kaul, E. W. Wong, L. Epp, B. D. Hunt, Nano Letters, 6, 942, 2006.
[7]M. B. Bryning, M. F. Islam, J. M. Kikkawa, A. G. Yodh, Advanced Materials, 17, 1186, 2005.
[8]Y. Yang, M. C. Gupta, K. L. Dudley, R. W. Lawrence, Nano Letters, 5, 2131, 2005.
[9] C. Xiang, Y. Pan, X. Liu, X. Sun, X. Shi, and J. Guo, Appl. Phys. Lett. **87**, 123103, 2005.
[10]C. J. Gannon, P. Cherukuri, B. I. Yakobson, L. Cognet, J. S. Kanzius, C. Kittrell, R. B. Weisman, M. Pasquali, H. K. Schmidt, R. E. Smalley, S. A. Curley, American Cancer Society, 110, 2654, 2007.
[11]B. Sitharaman, L. J. Wilson Journal of Biomedical Nanotechnology, 2007, 3, 342-352.
[12]D. Kajfez and P. Guillon (editors), Dielectric Resonators, Artech House, Dedham, MA 1986.
[13]QWED, http://www.qwed.com.pl, J. Baker-Jarvis, R. G. Geyer, J. H. Grosvenor, Jr., M. D. Janezic, C. A. Jones, B. Riddle, C. M. Weil, J. Krupka, IEEE Transactions on Dielectrics & Electrical Insulation, 5, 571, 1998.
[14]Parka, J., J. Krupka, R. Dąbrowski, and J. Wosik, J. of European Ceramic Society, 27, 2903, 2007.
[15]H. E. Bussey, IEEE Tr. on Instr. and Meas., IM-29, 120, 1980.
[16]J. Baker–Jarvis, M. D. Janezic, C. A. Jones, IEEE Tr. on Instrumentation and Measurements, 47, 338, 1998.
[17]C. Darne, L. –M. Xie, D. Padmaraj, P. Cherukuri, W. Wosik and J. Wosik, Materials Research Society Symposium Proceedings, 1057E, 1057-II15-61, 2008.
[18]H. Xu, S. M. Anlage, L. Hu, G. Gruner, Applied Physics Letters, 90, 183119, 2007.